energies

MDPI

Review

Part-I: State-of-the-Art Technologies of Solar Powered DC Microgrid with Hybrid Energy Storage Systems-Architecture Topologies

Dogga Raveendhra [1], Rajana Poojitha [2], Beeramangalla Lakshminarasaiah Narasimharaju [3], Aliona Dreglea [4], Fang Liu [5], Daniil Panasetsky [4], Mukesh Pathak [6] and Denis Sidorov [4,*]

1 EEE Department, Gokaraju Rangaraju Institute of Engineering and Technology, Hyderabad 500090, India
2 Zunik Energies Pvt. Ltd., I-2, TIDES Business Incubator, IIT Roorkee, Roorkee 247667, India
3 EEE Department, NIT Warangal, Warangal 506004, India
4 Applied Maths Department, Energy Systems Institute of Siberian Branch of Russian Academy of Sciences, 664033 Irkutsk, Russia
5 School of Automation, Central South University, Changsha 410083, China
6 EE Department, Indian Institute of Technology Roorkee, Uttarakhand 247667, India
* Correspondence: dsidorov@isem.irk.ru

Abstract: In the case of microgrid (MG) systems, the choice of the right configuration plays a vital role to meet grid/load necessities when integrating low voltage, non-linear and highly sensitive (to environmental conditions) power sources such as solar PV modules, batteries and supercapacitors (SCs), etc. In the case of MG systems, the choice of the right configuration and the appropriate type of power converters in any application can have a significant impact on the optimum performance. Numerous architectures have been proposed for the integration of various energy sources to achieve optimum performance. A large number of research articles have been published in these areas. In this article, the detailed organization of various architectures based on the arrangement of various sources and detailed analyses is presented along with a discussion on those architectures. Moreover, the suitability of all the reviewed architectures based on driving factors such as (a) high conversion gain, (b) good power decoupling, (c) high efficiency, (d) isolation, (e) power-handling capabilities and (f) compact design is presented in the discussions section. The critical examination and comparative study presented in this work can assist both industry personnel and academicians in selecting the best architectural and power converter topologies required for optimum performance.

Keywords: solar PV systems; hybrid energy storage systems; supercapacitors and batteries

Citation: Raveendhra, D.; Poojitha, R.; Narasimharaju, B.L.; Dreglea, A.; Liu, F.; Panasetsky, D.; Pathak, M.; Sidorov, D. Part-I: State-of-the-Art Technologies of Solar Powered DC Microgrid with Hybrid Energy Storage Systems-Architecture Topologies. *Energies* **2023**, *16*, 923. https://doi.org/10.3390/en16020923

Academic Editor: Antonio Lecuona

Received: 24 December 2022
Revised: 4 January 2023
Accepted: 7 January 2023
Published: 13 January 2023

1. Introduction

Communities in remote regions are completely isolated from the main grid because of decentralization and low populations [1,2]. Therefore, it is usually hard to attain electrification from the main grid in those areas due to financial restrictions and available resources. To address those restrictions, researchers came up with an alternative solution by utilizing sustainable energy sources (PV systems, solar thermal energy, wind energy, hydro, biomass, geothermal, ocean wave and tidal energy) and supportable storage technologies (batteries, SCs and fuel cells, etc.) due to the developments in power converter technologies and named it an autonomous distributed power system. Among all of these energy sources, the solar PV system has become the most common renewable energy (RE) technology in the current scenario, credited to its easy installation, advanced technology, low functional cost and modularity [3]. In general, PV systems offer a power supply for residential customers to fulfill their basic electricity requirements such as cooking, lighting, refrigeration and other critical electrical functions in two ways: on-grid and off-grid systems [4]. The common autonomous PV system model is shown in Figure 1, which is the more popular

way of supplying energy in remote areas. The MPPT controller in solar PV systems is an essential unit to achieve higher efficiency [5]. Moreover, for uninterrupted power to loads, the combination of energy storage systems (ESS) along with the solar PV unit is necessary because of the non-linear electrical characteristics of the PV array and the irregular nature of solar irradiation and temperature.

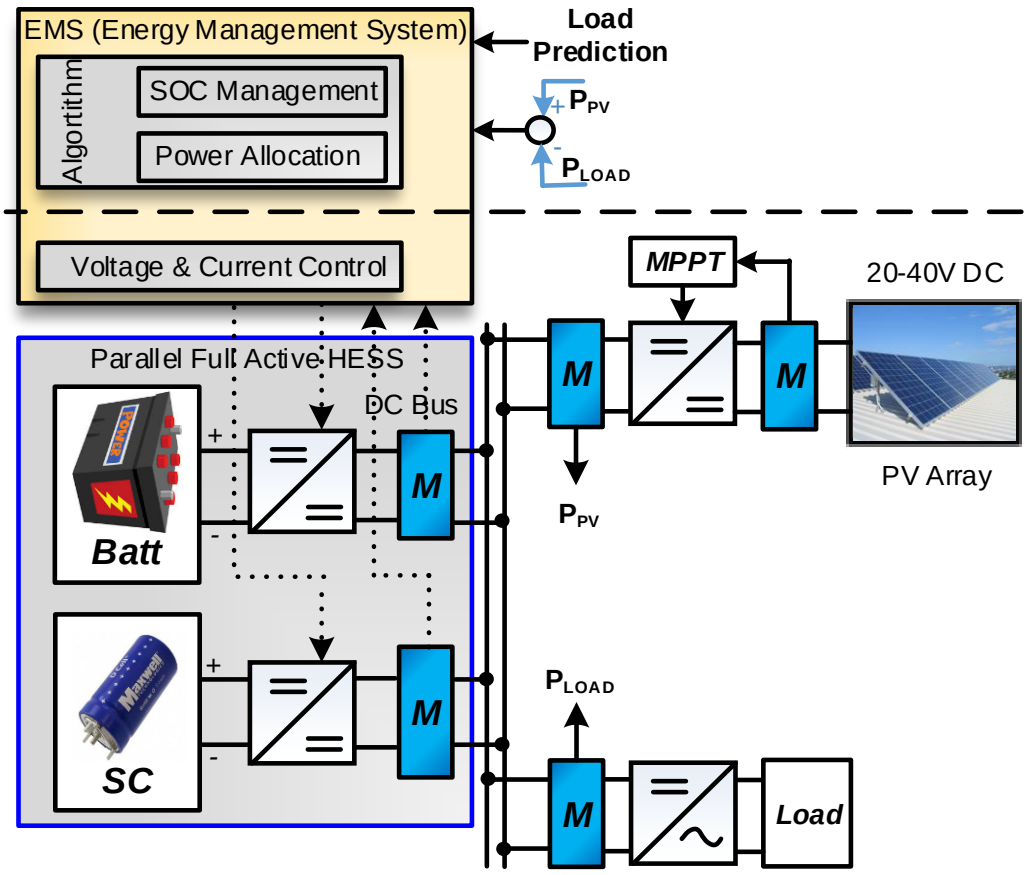

Figure 1. Typical autonomous PV-HESS grid system for rural electrification.

Most popular ESS technologies use a combination of lead-acid and lithium-ion (Li-ion) batteries [6]. The Li-ion type of battery has a better round trip efficiency, large energy density and extended life cycle when compared to LA batteries. However, these Li-ion batteries have the disadvantages of comparatively high cost and underdeveloped technology in bulk packaging. Conversely, for remote area electrification, LA batteries are more appropriate due to their improved thermal stability, and they are cheap when compared to Li-ion batteries. These LA batteries in the standalone PV system face additional stresses because of charge-discharge cycles due to the intermittent nature of solar energy, leading to decreased battery life [7,8]. Therefore, the concept of hybridization in various ESS technologies has become a more attractive and efficient way to minimize battery stresses by diverting the transient power variations to another energy storage (ES) element such as SC [9–11]. The SC stores electrical energy in a static field form through electrons and has more power density, shorter charging/discharging times and an almost infinite life cycle [12]. Dynamic power sharing is applicable in the battery–SC hybrid energy storage system (HESS) by separating the net demanded current into low-frequency and high-frequency components with the adoption of suitable power-sharing methods. In this, the nominal current component profile (low-frequency component) is supplied by the primary ESS device (battery bank). In contrast, the SC absorbs high-frequency components of power due to irregularities in solar power and load variations. Therefore, the stresses on the battery due to its high-frequency components are reduced, which results in an increase in the cycle number of the battery.

In the last few decades, for the integration of all the above-mentioned sources, different types of HESS architectures and energy management methods have been developed by researchers and are considered in this literature review [13–18]. In general, these HESS systems are proposed not only for remote power supply application but also in other applications such as electric vehicles, smart-grids, large-scale utilities and other high-power applications, which are considered in this review due to their suitability for this application as well. These systems need comprehensive sensing, calculation and communication, which increase complexity and create further problems in implementation. However, the HESS study presented in the literature so far for Microgrid applications, specifically in remote area electrification applications, is inadequate to select the right kind of architecture and suitable converter.

Furthermore, the most exciting research area for the integration of various electrical sources such as RE sources and ESS, specifically solar, batteries and SCs, is the recent trend of power electronics, including the study of bidirectional power converters. Bidirectional power converters differ from traditional unidirectional converters in that power can flow in both directions. Because of their flexibility, BDCs are used in microgrid systems to connect the aforementioned sources [19–21]. The BDC improves system performance and efficiency by interconnecting with power and ES devices, as it eradicates the need for a couple of separate unidirectional converters for bidirectional power flow. The typical structure of the BDC is depicted in Figure 2 [22]. The placement of the ESSs and their voltage levels determine the mode of converter operation (buck or boost mode), and the controller must be developed to control the system's current/voltage. In forward manner, the BDC is required to feed battery power to the load during transient and overload conditions, while in reverse mode it charges the battery pack [23]. As a result of their importance in electrical systems, this paper examines various power converters in various aspects.

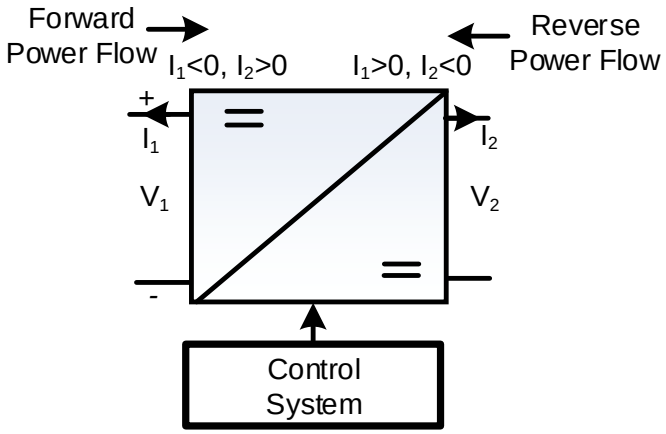

Figure 2. Structure of Bidirectional DC-DC converters (BDC).

The main goal of this paper is to fill the gap in the literature by providing an extensive review and analysis of the possible architectures, power management schemes of HESS and suitable power converter topologies for electrification for remote area application. The goals of this paper are to present the up-to-date HESS architecture and power converter topologies, which are reported in the literature in a systematic fashion. The manuscript also describes the classification of BDC topologies (non-isolated and isolated), which can help decide the potential BDC structure to be used for a particular HESS configuration. It is expected that the investigation will eventually help expedite the concept of HESS for application in some remote autonomous PV system applications, which will lead to a reduction in local residents' financial burden by adopting suitable architecture, converters, etc., to meet various objectives such as enhanced battery life, reliability, compactness, safety and efficiency, etc.

This paper is planned as follows: Section 2 describes the HESS literature review on various battery-SC HESS architectures with the mathematical models and their power allocation strategies for the study of the conventional autonomous PV grid system. The next subsections deal with various BDC topologies, along with the discussion of their classifications, their control and their switching strategies. For clear understanding, the layout of every category is explained in its own subsection. Section 3 discusses the overall comparison of the topologies and HESS configurations for the selection of the optimal topology for the specified application. Section 4 focuses on the trends in recent developments in MG systems. Concluding remarks are given in Section 5.

2. Architectures and Converter Topologies for Solar-Powered HESS

In only a few decades, the PV-powered DC microgrid research and manufacturing industries have developed at a breakneck rate. Despite the fact that many architectures and topologies have been created by researchers over the years, only a few promising approaches have been recognized by industries for stand-alone applications based on factors such as structure, efficiency, protection, reliability and cost, etc. As a result, the focus of this paper is on presenting a thorough overview of architectures and topologies that can serve as a useful guide for future study, as well as a collection of appropriate units to achieve the desired results. Various features such as the number of stages between the source and the load, isolation, power handling capability, output quality, voltage gain, interface type (grid/standalone) and soft/hard switching are investigated in this paper. However, for a better presentation, this analysis of technologies is divided into categories based on functionality, as shown in Figure 3, and then subdivided based on the above-mentioned attributes.

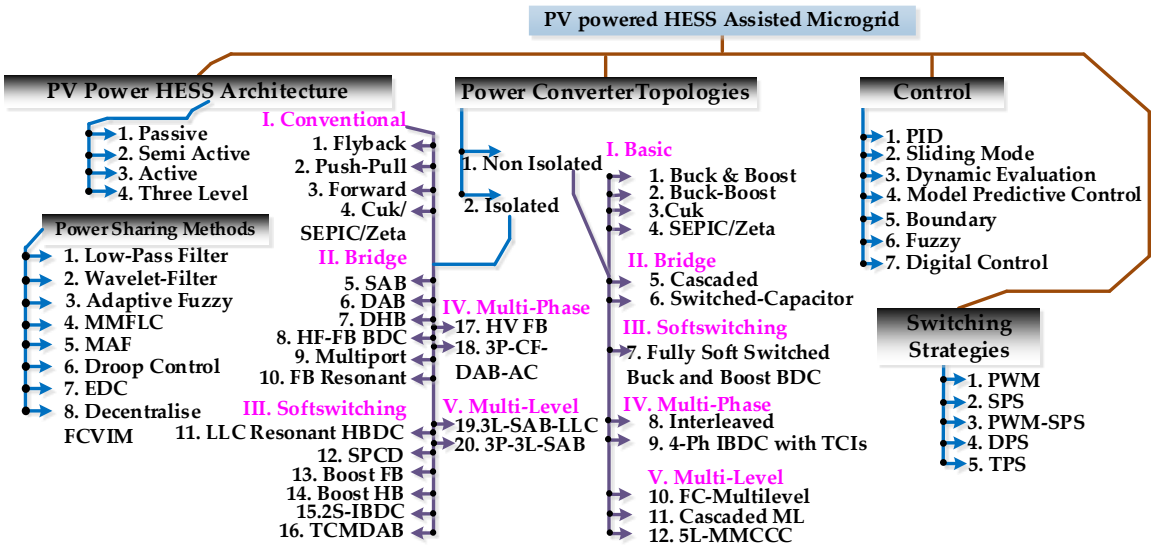

Figure 3. Classification of PV-powered HESS-Assisted Microgrid.

2.1. Hybrid Energy Storage System Architectures

For the best utilization of the various ESS elements, various battery-SC HESS configurations have been recommended in various applications [24]. As shown in Figure 4, all types of current or upcoming HESS configurations can be categorized based on the ESS count, power allocation methods among ESS components and interfacing strategies. Battery-SC based HESS can be organized in passive, semi-active, full-active, or their series and/or parallel combinations. In the passive HESS arrangement, the ESS terminals are immediately coupled to the DC bus, where the power allocation process and responses are decided by the electrical characteristics of the ESS elements. Contrarily, active elements, such as BDC power converters, are used in active HESS topologies to interconnect the ESS components with the DC bus and also control the power flow in an active manner. The

basic battery-SC-based HESS is depicted in Figure 4a, with both the battery and the SC accessing the same DC bus. No active elements are added to this configuration so that the time constants of the devices decide the power-sharing among ESS elements. The key drawback of this design is that SC power is not fully utilized. The distinct ESS elements in the passive HESS configuration possess different voltage levels at the common DC bus, so it is difficult to utilize the entire capacity of the SC, which results in low volumetric efficiency and the loss of the design flexibility of HESS. This is the primary topology of HESS and is not generally preferred in practical applications [25–27].

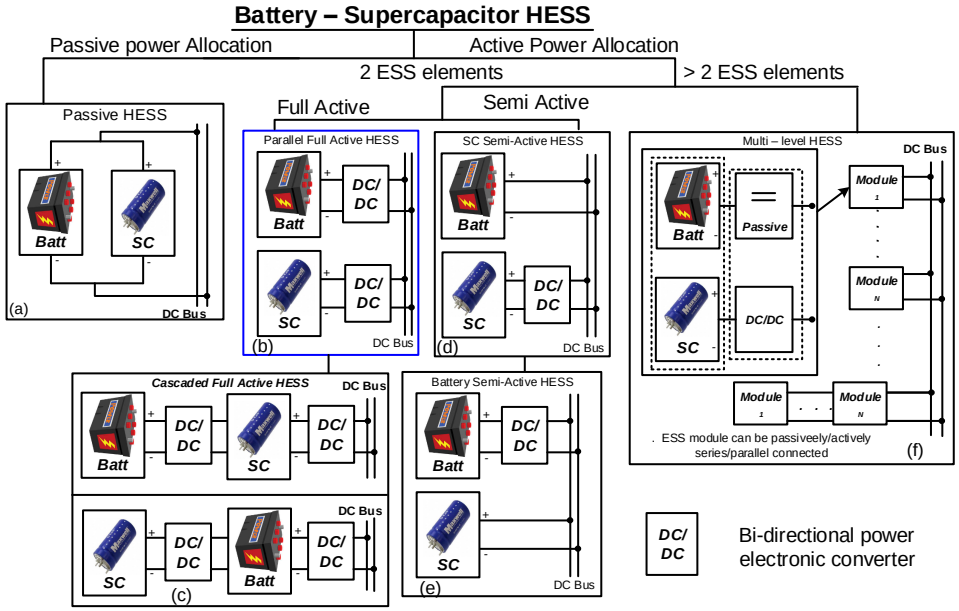

Figure 4. Classification of HESS architectures.

The active power flow control among ESS devices can be achieved by interfacing the separate ESS device with the DC bus through the suitable BDC, allowing more flexible settings for system arrangement. The actively controlled ESS units can be configured either in shunt (Figure 4b) or cascaded (Figure 4c). A full-active topology attains a better control effect than passive topology. However, it will increase the design complexity, efficiency and cost of the system. While achieving the DC bus voltage regulation, the power flow is controlled in the parallel fully active HESS topology by allotting the independent BDC to each ESS device. Both the ESS components operate with distinct voltages, which are isolated from the DC bus. Due to this advantage, the parallel full-active HESS topology is extensively reviewed and expanded by the researchers with distinct energy management algorithms [28–30]. In contrast, in the cascaded full-active HESS, as illustrated in Figure 4c, the battery and SC are connected in series, and the two DC-DC converters are cascaded with their corresponding ESS elements and are controlled with distinct voltage ratings. Due to this, the design complexity of the controller is increased. Generally, the main advantage in full-active HESS is that the control of power flow in every individual ESS component can be easily achieved, depending on the design of the power allocation strategy. However, it suffers from the initial cost and the robustness of the system. Because all ESS components are interconnected with DC-DC converters, the required rating of the electronic power elements is typically high for various ES applications such as residential energy systems and electric vehicles. This leads to a high increment in the overall cost of the system. Because of similar reasons, full-active systems that are used in PV systems entirely depend on BDCs and the related control model to guarantee reliable operation.

To obtain the advantages of both passive and full-active HESS topologies with less cost, semi-active HESS topologies, as depicted in Figure 4d,e, have been recommended to reduce the drawbacks of the above-mentioned two topologies [31]. The SC unit in the SC

semi-active HESS (Figure 4d) is regulated by utilizing a BDC and the battery unit is directly coupled to the DC bus. In this arrangement, the SC is permitted to change its terminal voltage in a wide range, which leads to enhanced volumetric efficiency. In many instances, the SC is used to absorb the high-frequency fluctuations that occur in the DC bus, whereas the directly coupled battery module will supply the required nominal demand. In such systems, during this steady-state situation, the DC bus voltage is maintained passively with minimum changes in the terminal voltage. Usually, the electrical characteristics of the battery are stable so that it improves the power system robustness. As in [32], it utilizes semi-SC HESS to avoid the adverse effects on the Li-ion battery in electric vehicles for the regular power transients.

On the other hand, the semi-active battery HESS (Figure 4e) connects the battery unit with the BDC, and the SC unit is directly coupled to the DC bus [33]. In this configuration, a large and unstable DC bus voltage is predicted due to the linear voltage-capacity characteristics of the SC, which may create problems in various applications. Additionally, the SC capacity is not fully utilized since it is passively connected to the DC bus, which decreases the volumetric efficiency. The setup of the SC should be sufficiently large to fulfill the vast range of the DC bus voltage.

On the other hand, another architecture named the multi-level HESS is reported in the literature, as shown in Figure 4f [34–36]. This architecture contains more than two ESS elements and is joined to the DC bus with/without DC-DC converters. A particular control strategy and power management system is implemented for a hybrid system configured with more than two ESS elements. It can be set up in various combinations, such as active and passive, either in parallel or in cascaded form. Based on various system demands to achieve better flexibility, the battery or SC is modularized to various power or voltage levels. The problem of imbalance occurring in every battery unit over numerous series-connected battery cells is eliminated by implementing a novel SC unit circuit, suggested by Ye et al. The novel SC cell with a battery HESS can be treated as an example; its topology as shown in Figure 4f [37]. This topology allows for a more flexible HESS with regard to system configuration, and for the wider energy and power applications this has the flexibility for a huge and complex energy management system. A detailed explanation, along with the mathematical expressions for each architecture, is presented in the following subsections.

2.1.1. Passive HESS

The equivalent circuit model is shown in Figure 5 [38] and represents the response of the passive HESS configuration, shown in Figure 4a.

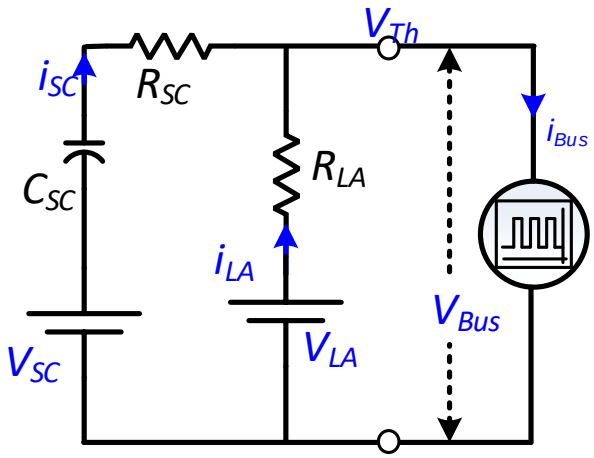

Figure 5. Equivalent model of the passive HESS configuration.

The *SC* is modeled with the series-connected equivalent resistance R_{SC}, a definite initial voltage V_{sc} and the huge value of capacitance C_{SC}, whereas the lead-acid battery is modeled with the series-connected equivalent resistance R_{LA} and a constant voltage source V_{LA}.

The representation of the equivalent Thevenin's circuit contains voltage $V_{Th}(s)$ and impedance Z_{Th}(s) and is shown in Figure 6 for the above equivalent passive HESS configuration of Figure 5 in the frequency domain (s-domain) using Thevenin's concept; it can be calculated as (here readers may also refer to [26,39] and references therein):

$$V_{Th}(s) = \frac{V_{LA}}{s} + \frac{V_{SC} - V_{LA}}{s + \frac{1}{\tau_p}} r_p \tag{1}$$

where $r_p = \frac{R_{LA}}{R_{LA}+R_{SC}}$, $\tau_p = (R_{LA} + R_{SC})C_{SC}$,

$$Z_{Th}(s) = r_p \times \frac{s + \frac{1}{R_{SC}C_{SC}}}{s + \frac{1}{\tau_p}} \tag{2}$$

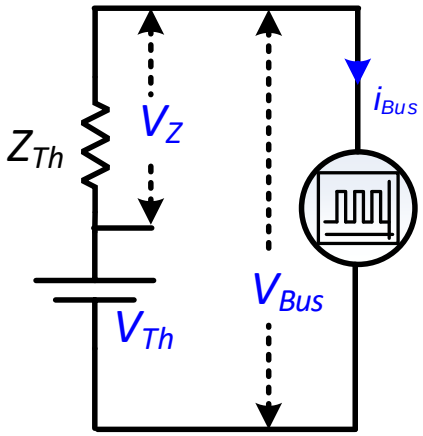

Figure 6. Thevenin's equivalent model of the passive HESS configuration.

Here, s denotes the complex variable. Let a continuous pulse current load be the input, the periodic load current, then $i_{Bus}(t)$ for the first N pulses can be expressed as follows:

$$i_{Bus}(t) = I_{Bus} \sum_{k=0}^{N-1} [\phi(t - kT) - \phi(t - (k + D)T)] \, (k = 0, 1, 2, \ldots) \tag{3}$$

Here, D is the pulse load duty ratio; $\phi(t)$ is the Heaviside step function. The corresponding voltage expression in the time domain (t-domain) is obtained as:

$$v_{Bus}(t) = V_{LA} + r_p(V_{SC} - V_{LA})e^{-\frac{t}{\tau_p}} - R_{LA}I_{Bus} \sum_{k=0}^{N-1} \begin{bmatrix} \left(1 - r_p e^{-\frac{t-kT}{\tau_p}}\right)\phi(t - kT) \\ -\left(1 - r_p e^{-\frac{t-(k+D)T}{\tau_p}}\right)\phi(t - (k + D)T) \end{bmatrix} \tag{4}$$

Hence, the current through the battery and the SC ($i_{LA}(t)$ and $i_{SC}(t)$) can be derived correspondingly as follows:

$$\begin{aligned} i_{LA}(t) &= \tfrac{V_{LA} - v_{Bus}(t)}{R_b} = -\tfrac{(V_{SC} - V_{LA})}{R_{LA}+R_{SC}} * e^{-\frac{t}{\tau_p}} + \\ & I_{Bus} \sum_{k=0}^{N-1} \left[\left(1 - r_p e^{-\frac{t-kT}{\tau_p}}\right)\phi(t - kT) - \left(1 - r_p e^{-\frac{t-(k+D)T}{\tau_p}}\right)\phi(t - (k + D)T) \right] \end{aligned} \tag{5}$$

$$i_{SC}(t) = i_{Bus}(t) - i_{LA}(t) \tag{6}$$

Under the steady-state conditions, the battery, *SC* and the *DC* bus will share the common terminal voltage, where $V_{SC} = V_{LA}$, then their steady-state currents can be obtained as:

$$i_{LAss}(t) = I_{Bus}\sum_{k=0}^{N-1}\left[\left(1 - r_p e^{-\frac{t-kT}{\tau_p}}\right)\phi(t-kT) - \left(1 - r_p e^{-\frac{t-(k+D)T}{\tau_p}}\right)\phi(t-(k+D)T)\right] \quad (7)$$

At instant $t = (D + k)T$, the resultant variation in the HESS current is obtained whenever the changes allow in the input pulsed load current. Consider the peak current appears when N tends to infinity, then the simplified battery peak current is expressed as follows:

$$i_{LAp} = I_{Bus}(1 - \varepsilon) \quad (8)$$

Here, parameter ε is defined as follows:

$$\varepsilon = \frac{R_{LA}}{R_{LA} + R_{SC}} * e^{-\frac{DT}{\tau_p}} * \frac{1 - e^{-\frac{(1-D)T}{\tau_p}}}{1 - e^{-\frac{T}{\tau_p}}} \quad (9)$$

The current distribution relationship between the *SC* and the battery is defined by the parameter ε. It means when the *SC* is available in the HESS systems, then the battery peak current rating is always less than the dc bus current I_{Bus}. The relation between the *DC* bus current and battery current at a particular time is expressed in Equation (11). The *DC* bus current obtained when the lead-acid battery operates under the rated current is:

$$I_{Bus} = \frac{1}{(1 - \varepsilon)} I_{LA\_rated} = \partial * I_{LA\_rated} \quad (10)$$

In order to estimate the maximum power improvement in HESS, the instantaneous maximum power of HESS at the rated current can be given as:

$$P_{HESSp} = I_{Bus} * V_{Bus} = \partial * I_{LA\_rated} * V_{Bus} = \partial * P_{LA\_rated} \quad (11)$$

As parameter ∂ in Equation (10) is always more than 1, hence the HESS maximum power is enhanced, with the *SC* passively connected in parallel. Figure 7 shows the incorporation of the passive battery-*SC* HESS on the standard standalone PV system. In general, the primary ESS element to be chosen is the *LA* battery. The modeling of the charge controller is made by employing a unidirectional DC-DC converter with a maximum power point tracking (MPPT) algorithm. For integrating the load, and HESS, a couple of control switches are used, which will be discussed in the later sections.

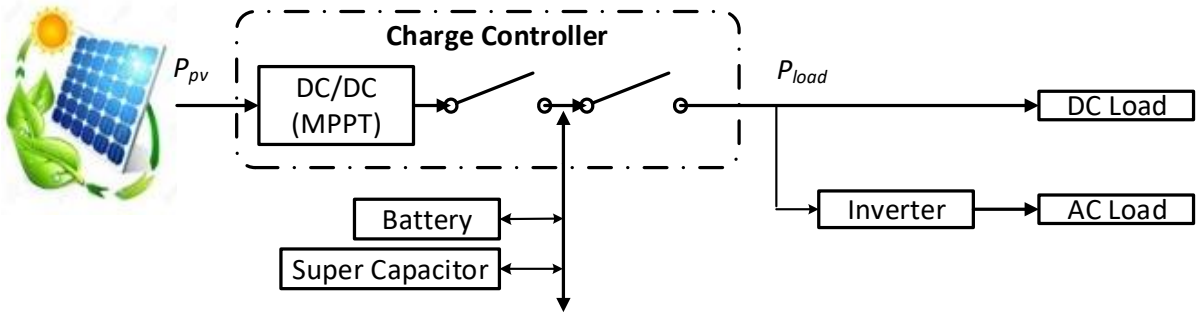

Figure 7. Passive HESS based autonomous PV grid.

2.1.2. Supercapacitor Semi-Active HESS

The equivalent circuit for the *SC* semi-active HESS (Figure 4d) in both time and *s*-domains is depicted in Figure 8. The DC-DC converter is shortened and denoted in terms of the parameters of voltage transfer rate κ_{sc} and efficiency η_{SC} by ignoring the dynamic

characteristics [39]. Therefore, the current and actual terminal voltage of the *SC* prior to the DC-DC converter can be expressed as:

$$i_{SC}(t) = \frac{\kappa_{SC}}{\eta_{SC}} i_C(t) = i_{Bus}(t) - i_{Bus}(t)_{LPF} \tag{12}$$

$$V_{SC} = \frac{V_C}{\kappa_{SC}} = \frac{V_{Bus}}{\kappa_{SC}} \tag{13}$$

where $i_{Bus}(t)_{LPF}$ is the filter output of $i_{Bus}(t)$.

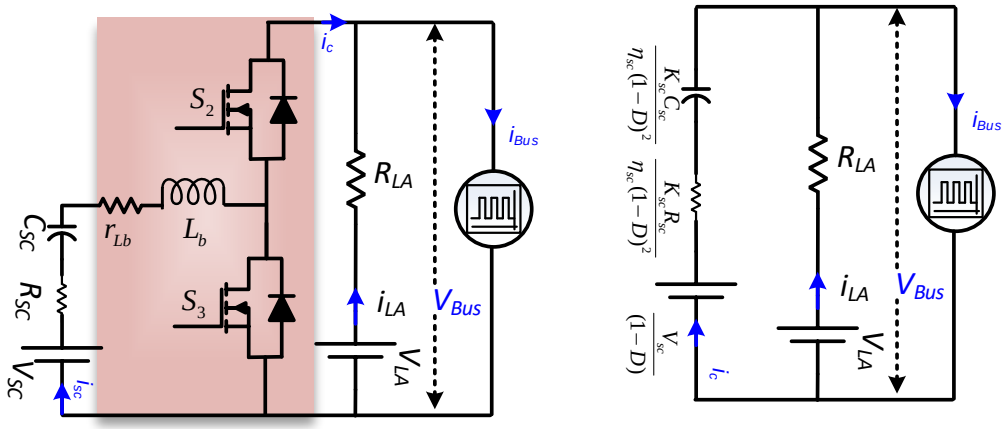

Figure 8. The *SC* semi-active HESS equivalent circuit.

The *SC* and battery currents on the *DC* bus are expressed when the input of the pulsed current load $i_{Bus}(t)$ is subjected as:

$$i_{Bus}(t) = I_{Bus} \sum_{k=0}^{N-1} [\phi(t - kT) - \phi(t - (k + D)T)] = i_C(t) + i_{LA}(t) \tag{14}$$

$$i_C(t) = \frac{\eta_{SC}}{\kappa_{SC}} i_{SC}(t) = \frac{\eta_{SC}}{\kappa_{SC}} [i_{Bus}(t) - i_{Bus}(t)_{LPF}] \tag{15}$$

$$i_{LA}(t) = I_{Bus} \sum_{k=0}^{N-1} [\phi(t - kT) - \phi(t - (k + D)T)] - \frac{\eta_{SC}}{\kappa_{SC}} [i_{Bus}(t) - i_{Bus}(t)_{LPF}] \tag{16}$$

where $\phi(t)$ is again the Heaviside step function. Consider the peak current produced at the end of the pulse duty ratio, $t = (k + D)T$, and then the extracted battery peak current can be written as:

$$i_{LAp} = I_{Bus} - \frac{\eta_{SC}}{\kappa_{SC}} [i_{Bus}(t) - i_{Bus}(t)_{LPF}] \tag{17}$$

It is observed that the *SC* current decreases the peak current of the battery due to active control through the DC-DC converter, which results in the reduction of the stresses on the battery caused by the pulsed currents.

In general, a low-pass filter is employed to segregate the low- and high-frequency components. To control the *SC* current flow, the high-frequency component is utilized. The reference signal is tracked by implementing a simple proportional-integral controller, while the lead-acid battery bank takes care of the rest of the current requirement. The response time constant can be modified for the optimal usage of the *SC* unit, which is the key advantage of actively controlled *SC* units. Moreover, a wider variation in *SoC* is allowed by connecting the *SC* unit through the BDC with the *DC* bus and thereby improves the volumetric efficiency significantly. The inrush currents are formed when there is a variation of load current in step fashion, which is due to the inevitable time delay of the active component and controller.

A similar autonomous PV system, along with the ES unit of the *SC* semi-active HESS, is depicted in Figure 9. In this scheme, the *SC* is interfaced with a BDC while the *LA* battery is connected passively to the *DC* bus formed by the Solar PV unit. The resultant error in the value of the current is taken into consideration to produce the proper PWM signal along with a suitable duty cycle D_{SC} by the controller in order to regulate the power distribution from the *SC*. An easier control method is shown in Figure 10, in which the low-pass filter filters the required power P_{HESS} component, and the *SC* circuit uses the remaining high-frequency component as a reference signal $P_{SC(\text{ref})}$. The PI controller (current tuning tracker) is utilized to control the power flow from the *SC*. When choosing the low-pass filter bandwidth, there is a need for compromise between the *SC* size and the smoothness of battery current I_{Batt}. For example, a smooth I_{Batt} is generated with comparatively low cut-off frequency in the low-pass filter. However, this demands a larger *SC* size and also more power rating of active elements in the DC-DC converter.

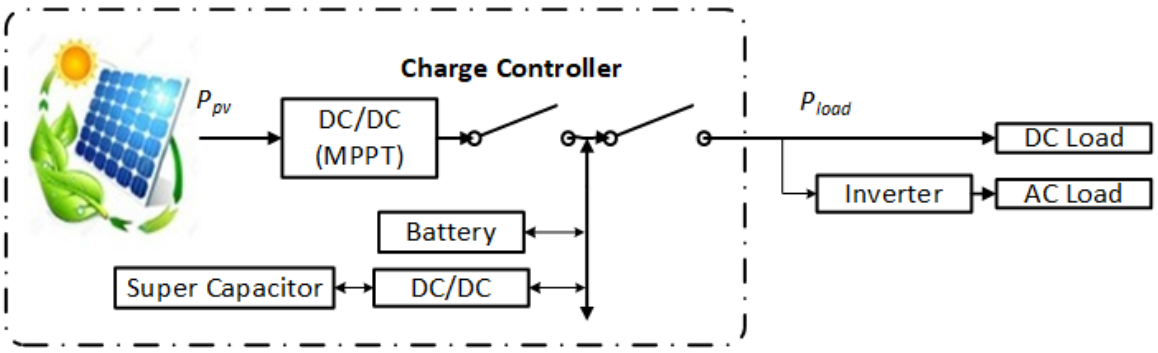

Figure 9. *SC* semi-active HESS supported autonomous PV system.

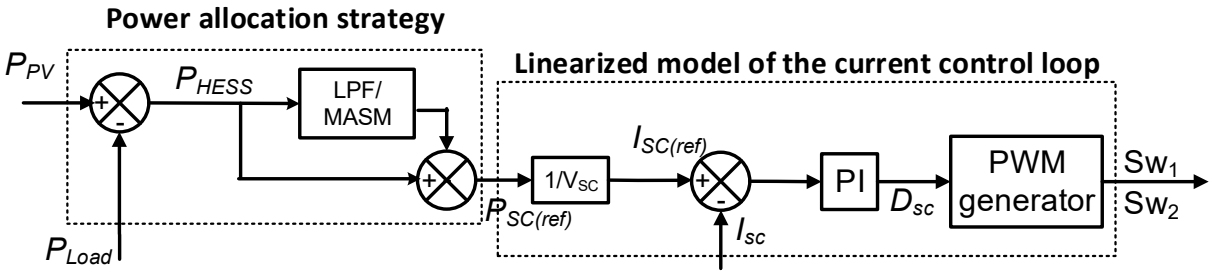

Figure 10. Power allocation scheme in *SC* semi-active HESS.

From the above discussion, the DC-DC converter in the *SC* semi-active HESS is coupled between the *SC* pack and the DC bus, as depicted in Figure 8.

Thus, the system efficiency η_{cs} can be written as a ratio of two Volterra integrals:

$$\eta_{cs} = \frac{\int_0^T (V_{LA} - i_{LA}R_{LA})i_{Bus}(t)dt}{\int_0^T (V_{SC}i_{SC} + V_{LA}i_{LA})dt} \tag{18}$$

2.1.3. Battery Semi-Active HESS

The equivalent circuit for the battery semi-active HESS (Figure 4e) in the time and frequency domain is shown in Figure 11. It is used to represent the battery unit including dynamics [40]. In this scheme, the *SC* is passively coupled to the load while the BDC is coupled between the battery unit and the load. The benefit of the battery semi-active HESS is that it does not have to adjust the battery unit voltage to the *DC* bus. The first order electrical circuit model is utilized for the system-level study to depict *SC* unit dynamics [41].

The open-circuit voltage (OCV) of the *SC* (V_{SC}) decides the capacitance of the *SC* pack. The internal resistance of the *SC* is represented as R_{SC}.

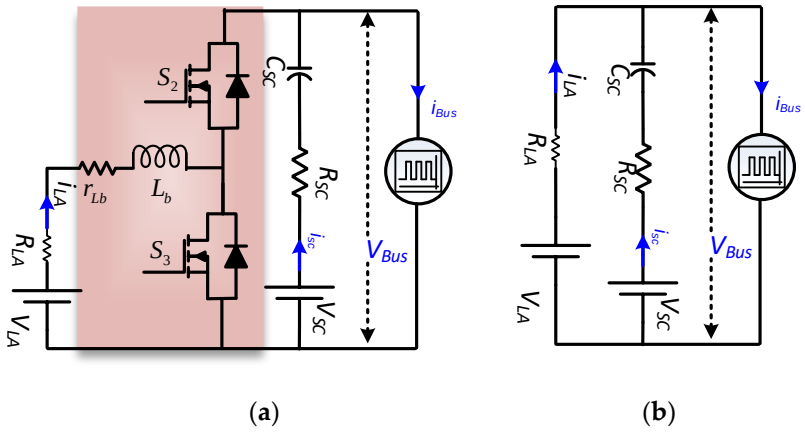

Figure 11. (**a**) Battery semi-active HESS circuit (**b**) equivalent circuit of (**a**).

2.1.4. Full-Active HESS

In full-active HESS, a couple of distinct BDCs are connected for interfacing the battery and *SC* banks to share the power between them with the DC bus. This will improve the flexibility of HESS and also enhances the performance of the entire system and life of the battery too. Two feasible configurations of this full-active HESS illustrated in Figure 4b,c are parallel full-active HESS and cascaded full-active HESS, respectively. Here, in Figure 12, parallel active topology is presented. Three feasible configurations of the full-active hybrid are described in [42–44]. In this, the first two configurations are advancements of the battery and *SC* semi-active schemes, whereas the last one combines both semi-active configurations to form an active one.

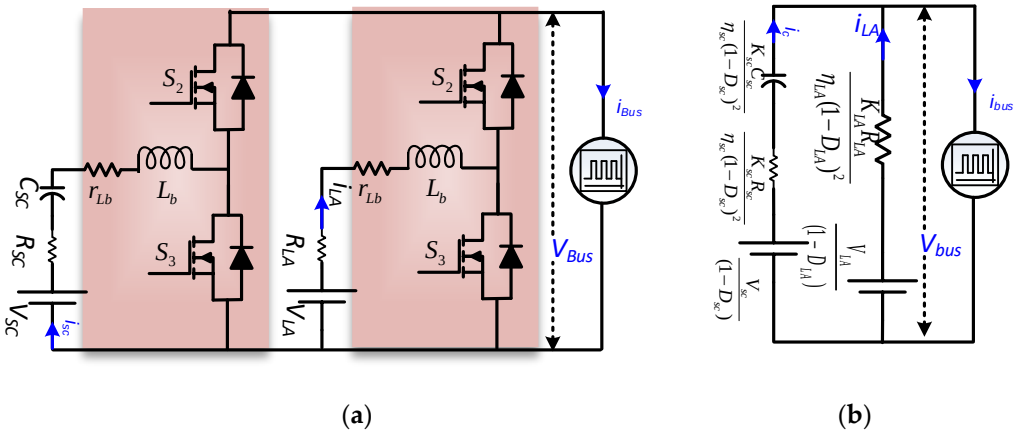

Figure 12. (**a**) full-active HESS (**b**) equivalent circuit.

In parallel active topology, the BDC converters decouple both the ESS elements from the *DC* bus, as illustrated in Figure 4a. This parallel active topology is most often used for storage system applications scaled to the DC Microgrid level, which permits full control over ESS components [45]. By adopting a proper control strategy, this topology can enhance the overall system performance, life of the battery and *DC* bus stability [46]. For example, the battery can be configured to provide the low-frequency power exchange, while the other ESS, the *SC*, which is a high-power density ESS device, is configured to react to the high-frequency power exchange. The voltage level isolation of both ESS components permits a broad operating range of *SOC*, which can enhance the HESS volumetric efficiency.

The cascaded structure, as depicted in Figure 4b, is the active topology, where the battery and *SC* are decoupled from the *DC* bus [42,47] by cascading a couple of DC-DC convert-

ers. The BDC, which is associated with the battery, is generally current-controlled to allow smooth power transfer from the battery. The transients during the charging/discharging process are caused due to the irregular nature of the solar power generation and load demands in remote areas. Hence, the BDC, which is connected to the *SC*, is usually voltage-controlled to manage the *DC* bus voltage by absorbing the high-frequency power fluctuations [48]. A large voltage operating range between the *SC* and *DC* bus is expected because the *SC* has a huge voltage operating range. Thus, the power loss increases in the BDC because the efficiency maintained over the wide range of operating voltages is quite difficult.

When the power converters in the system increase, the total coulombic efficiency of the HESS reduces because of losses in all the power converters; therefore, the reliability of the BDC and the control strategy decide the performance of the HESS system.

Thevenin's equivalent voltage and impedance (V_{Th}(s) and Z_{Th}(s)) in the above equivalent full-active HESS configuration in the *s*-domain and *t*-domain are:

$$\begin{aligned} V_{Th}(t) = & \frac{V_{LA}}{(1-D_{LA})\left(1+\frac{V_F}{V'_{LA}}+\frac{D_{LA}r_{DS}+(1-D_{LA})R_F+r_L}{(1-D_{LA})^2R_L}\right)} \\ & + \frac{R_{LA}m_{SC}}{m_1} \times \left(\frac{V_{SC}}{(1-D_{SC})x_{SC}} - \frac{V_{LA}}{(1-D_{LA})x_{LA}}\right)e^{-\frac{m_{LA}}{C_{SC}m_1}t} \end{aligned} \tag{19}$$

$$Z_{Th}(t) = \left(\frac{R_{LA}m_{LA}C_{SC}m_{SC}}{m_1}\right)^2 \times \exp^{\left(-\frac{m_{LA}}{C_{SC}m_1}t\right)} + \left(\frac{R_{sc}R_{LA}}{Rm_1}\right)\delta(t) \tag{20}$$

Here, $m_1 = R_{LA}(1-D_{SC})^2(x_{SC})^3 + R_{SC}(1-D_{LA})^2(x_{LA})^3$, $m_{LA} = (1-D_{LA})^2(x_{LA})^3$ and

$$m_{SC} = (1-D_{SC})^2(x_{SC})^3 \tag{21}$$

$$\begin{aligned} V_{Bus}(t) = & \frac{V_{LA}}{(1-D_{bat})\left(1+\frac{V_F}{V'_{LA}}+\frac{D_{LA}r_{DS}+(1-D_{LA})R_F+r_L}{(1-D_{LA})^2R_L}\right)} \\ & + \frac{R_{LA}m_{LA}}{m_1}\cdot\left(\frac{V_{LA}}{(1-D_{LA})x_{LA}} - \frac{V_{SC}}{(1-D_{SC})x_{SC}}\right)e^{-\frac{m_{LS}}{C_{SC}\times m_1}t} \\ & - \frac{I_{Bus}R_{LA}}{m_{LA}}\sum_{k=0}^{N-1}\left[\begin{array}{l} \left(1-e^{-\frac{(t-kT)m_{LA}}{C_{SC}\times m_1}}\left(\frac{R_{LA}m_{SC}}{m_1}\right)\right)\phi(t-kT) \\ -\left(1-e^{-\frac{m_{LA}(t-(k+D)T)}{C_{SC}\times m_1}}\left(\frac{R_{LA}m_{SC}}{m_1}\right)\right)\phi(t-(k+D)T) \end{array}\right] \end{aligned} \tag{22}$$

Now, the voltage at the terminals of the active HESS in the t-domain can be expressed, as shown in Equation (22). Hence, the current through the battery and the *SC* ($i'_{LA}(t)$ and $i'_{SC}(t)$) can be derived as:

$$\begin{aligned} i'_{LA}(t) = & -\left[\begin{array}{l} e^{-\frac{m_{LA}}{C_{SC}m_1}t} \times \left(\frac{V_{LA}}{(1-D_{LA})x_{LA}} - \frac{V_{SC}}{(1-D_{SC})x_{SC}}\right) \\ \times \frac{m_{LA}m_{SC}}{m_1} \end{array}\right] \\ & + I_{Bus}\sum_{k=0}^{N-1}(\phi(t-kT) - \phi(t-(k+D)T)) - \left[\begin{array}{l} \frac{R_{LA}m_{SC}I_{Bus}}{m_1}\times \\ \sum_{k=0}^{N-1}\left(\begin{array}{l} e^{-\frac{m_{LA}(t-(k+D)T)}{C_{SC}m_1}}\phi(t-(k+D)T) \\ -e^{-\frac{m_{LA}(t-kT)}{C_{SC}m_1}}\phi(t-kT) \end{array}\right) \end{array}\right] \end{aligned} \tag{23}$$

$$\begin{aligned} i'_{sc}(t) = & -\left[e^{-\frac{m_{LA}}{C_{SC}m_1}t} \times \frac{[m_{SC}m_{LA}]}{m_1}\left(\frac{V_{LA}}{(1-D_{LA})x_{LA}} - \frac{V_{SC}}{(1-D_{SC})x_{SC}}\right)\right] \\ & + \left[\frac{R_{LA}m_{SC}I_{Bus}}{m_1}\sum_{k=0}^{N-1}\left(\begin{array}{l} e^{-\frac{(m_{LA}(t-(k+D)T)}{C_{SC}m_1}}\phi(t-(k+D)T) \\ -e^{-\frac{m_{LA}(t-kT)}{C_{SC}m_1}}\phi(t-kT) \end{array}\right)\right] \end{aligned} \tag{24}$$

Under steady state conditions, the battery, the *SC* and the *DC* bus will distribute common terminal voltage, where $V_{SC} = V_{LA}$, then their steady-state currents are obtained as:

$$i'_{LAss}(t) = I_{Bus}\sum_{k=0}^{N-1}(\phi(t-kT) - \phi(t-(k+D)T)) - \left[\frac{R_{LA}m_{SC}I_{Bus}}{m_1}\sum_{k=0}^{N-1}\begin{pmatrix} e^{-\frac{m_{LA}(t-(k+D)T)}{C_{SC}m_1}}\phi(t-(k+D)T) \\ -e^{-\frac{m_{LA}(t-kT)}{C_{SC}m_1}}\phi(t-kT)\end{pmatrix}\right] \quad (25)$$

$$i'_{scss}(t) = \frac{R_{LA}m_{SC}I_{Bus}}{m_1}\sum_{k=0}^{N-1}\begin{pmatrix} e^{-\frac{m_{LA}(t-(k+D)T)}{C_{SC}m_1}}\phi(t-(k+D)T) \\ -e^{-\frac{m_{LA}(t-kT)}{C_{SC}m_1}}\phi(t-kT)\end{pmatrix} \quad (26)$$

At instant $t = (D + k)T$, the resultant variation in the HESS current is obtained whenever the changes allow in the input pulsed current load. Consider the peak current appears when N tends to infinity, then the simplified battery peak current is expressed as:

$$i'_{LAp} = I_{Bus}(1-\varepsilon) \quad (27)$$

where

$$\varepsilon = \frac{R_{LA}m_{SC}}{m_1}e^{-\frac{m_{LA}DT}{m_1}} \times \left(\frac{1-e^{-\frac{m_{LA}(1-D)T}{C_{SC}m_1}}}{1-e^{-\frac{m_{LA}T}{C_{SC}m_1}}}\right) \quad (28)$$

The current distribution relationship between the *SC* and battery is defined by the parameter ε. That means when the *SC* is connected, then I_{Bus} is always greater than the battery peak current.

2.1.5. Three-Level HESS

The three-level HESS configuration is proposed in [49] to improve the advantages of the former two (passive and semi-active) topologies. Figure 13 represents the equivalent circuits of the present circuit. The terminal voltage and current of the *SC* are expressed as follows:

$$V_{SC} = \frac{V_C}{\kappa_{SC}} = \frac{V_{Bus}}{\kappa_{SC}} \quad (29)$$

$$i_{SC}(t) = \frac{\kappa_{SC}}{\eta_{SC}}i_C(t) = i_{Bus}(t) - W_1 * i_{Bus}(t)_{LPF1} - \{[i_{Bus}(t) - w_1 * i_{Bus}(t)_{LPF1}]\}_{LPF2} \quad (30)$$

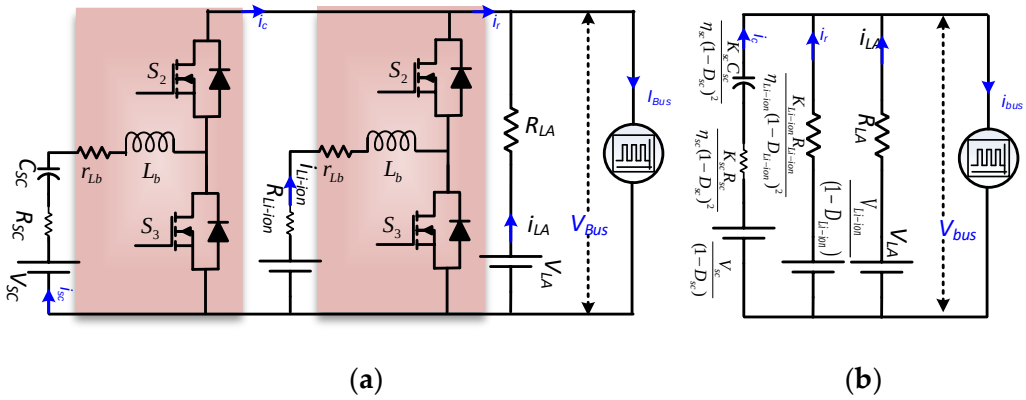

Figure 13. (**a**) Three-level HESS equivalent circuit (**b**) equivalent circuit of (**a**).

Moreover, the similar expressions for the *Li-ion* battery are:

$$V_{Li-ion} = \frac{V_r}{\kappa_{Li-ion}} = \frac{V_{bus}}{\kappa_{Li-ion}} \tag{31}$$

$$i_{Li-ion}(t) = \frac{\kappa_{Li-ion}}{\eta_{Li-ion}} i_r(t) = \{[i_{Bus}(t) - w_1 * i_{Bus}(t)_{LPF1}]\}_{LPF2} \tag{32}$$

Here, the voltage gains and efficiencies of the respective DC-DC converters are η_{SC}, η_{Li-ion}, κ_{sc} and κ_{Li-ion}, respectively. w_1 is the scaling factor that sets the proportion of the capacity of the *Li-ion* battery in the total power requirement. The lead-acid battery, pulsed current input, *SC* and *Li-ion* battery currents for the pulse load response are as follows:

$$i_{LA}(t) = I_0 \sum_{k=0}^{N-1} [\phi(t - kT) - \phi(t - (k + D)T)] = \frac{\eta_{SC}}{\kappa_{SC}} i_{SC}(t) - \frac{\eta_{Li-ion}}{\kappa_{Li-ion}} i_{Li-ion}(t) \tag{33}$$

$$i_{Bus}(t) = I_{Bus} \sum_{k=0}^{N-1} [\phi(t - kT) - \phi(t - (k + D)T)] = i_{LA}(t) + i_r(t) + i_C(t) \tag{34}$$

$$i_C(t) = \frac{\eta_{SC}}{\kappa_{SC}} i_{SC}(t) \tag{35}$$

$$i_r(t) = \frac{\eta_{Li-ion}}{\kappa_{Li-ion}} i_{Li-ion}(t) \tag{36}$$

The *Li-ion* battery is allowed to respond to the medium frequency component, whereas the *SC* is set to respond for transient current fluctuations and also to supply some part of the demanded current. This helps to reduce the maximum current in the passive lead-acid battery bank, and results in increasing the battery life cycle.

The three-level battery-*SC* HESS supported autonomous PV grid system is shown in Figure 14, where three distinct ESS elements are used to achieve improvement in the reduction of stresses. In this configuration, two complementary ESS devices (*Li-ion* and *SC*) with active control are connected in shunt along with a direct-coupled primary lead-acid battery. With this combination of *Li-ion* units and *SC*, the capability of stress reduction is enhanced by managing a wider spectrum of current variation and also supplies some portion of the required nominal current. This allows for the most stable charge-discharge operation and reduces the maximum current in the primary lead-acid battery bank.

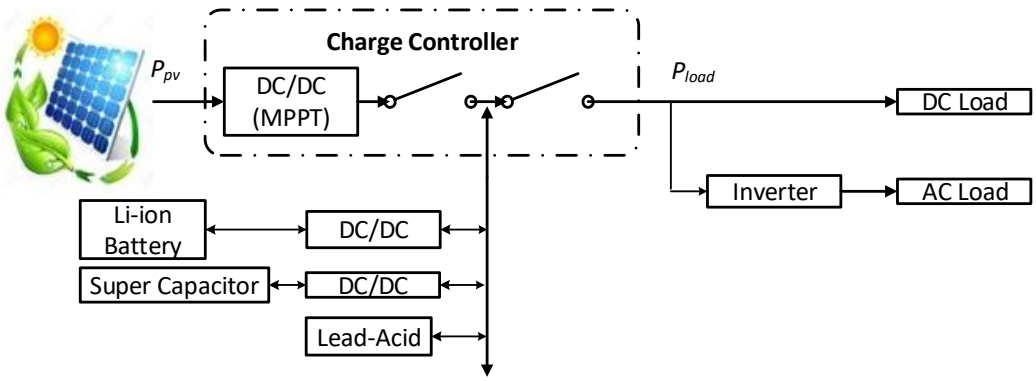

Figure 14. Autonomous PV grid system with three-level HESS.

Figure 15 shows the related power-sharing method, where the net power demand is separated into three frequency ranges by cascading two low-pass filters. The high-frequency component $P_{SC}(ref)$ is used as a reference signal for the *SC* to control its power flow, whereas the *Li-ion* module uses the medium-frequency component $P_{Li\text{-}ion(ref)}$ as reference. The part of the load from the total power demand to be handled by the *Li-ion* module is decided by the proper selection of scaling factors w_1.

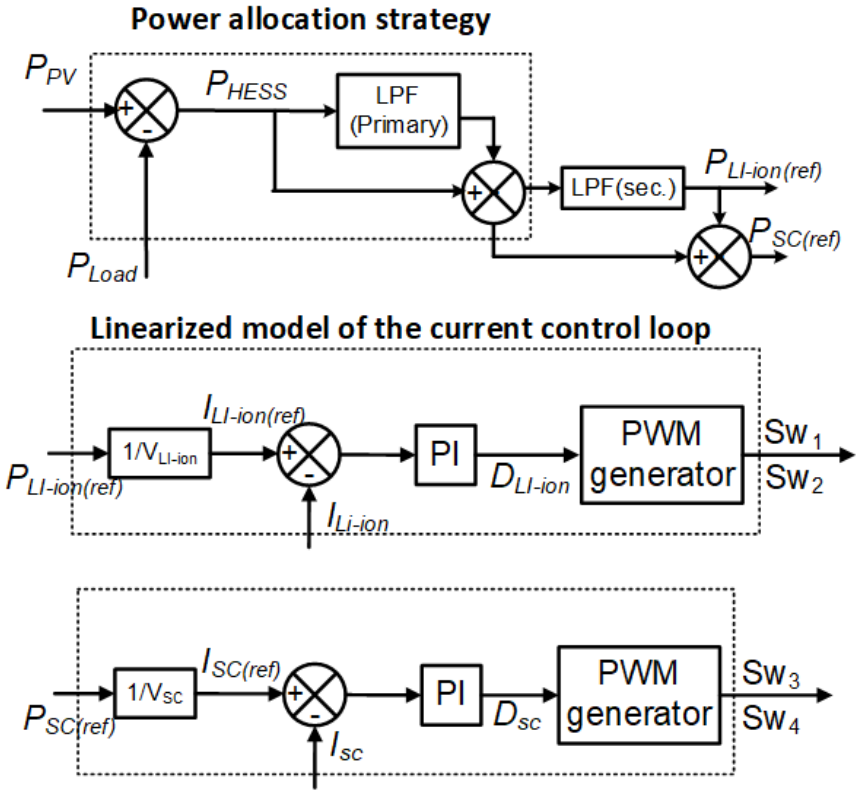

Figure 15. Power-sharing technique in three-level HESS.

So far, a detailed review of distinct HESS topologies and the role of the BDC in these topologies have been discussed. In this context, it is also essential to discuss various BDC configurations, control schemes and switching strategies, described in the following sections.

3. Discussion

A. *Discussion on HESS Architectures*

Depending on the requirement, the battery-*SC* HESS topologies and energy distribution techniques are varied with regards to their performance, control complexity and cost. This paper presented various HESS architectures used in the autonomous PV grid system, particularly for the application of electrification in rural areas. Many of the autonomous PV-based power systems for electrification in rural areas are graphically isolated when compared to some other high-power applications. Because of the high maintenance cost and restricted technical support, system robustness is one of the most important issues, and that should be considered while designing HESS. Therefore, full-active HESS configurations may not be the best candidates for use in rural electrification applications in terms of reliability compared to multi-level HESS. Contrarily, the preferred option in terms of complexity is the primary energy management implemented with the least number of active elements integrating the auxiliary ESS unit(s). From all the above discussed HESS topologies, the five possible configurations for autonomous PV-powered rural electrification are the passive HESS (Figure 4a), full-active HESS (Figure 4b), *SC* semi-active HESS (Figure 4d), battery semi-active HESS (Figure 4e) and multi-level HESS topologies (Figure 4f) with directly coupled primary ESS.

The comparison table for all the discussed HESS architectures is shown in Table 1, where various features are differentiated for selecting the best possible configuration of HESS in several applications such as EVs, HEVs, DCMG, etc. By comparing all the features, the *SC* semi-active configuration can be treated as the best optimal solution in consideration of cost, *SC* utilization, efficiency and design complexity.

Table 1. Features of various HESS architectures.

Features	Passive HEES	Battery Semi-Active HESS	SC Semi-Active HESS	Full-Active HESS	Multi-Level HESS
Figure	4a	4e	4d	4b,c	4f
Reference	[26,38]	[41,49]	[39,40,49]	[42–44]	[49]
Required no. of BDC converters	-	1	1	2	Depending on the level of HESS
Volumetric Efficiency of *SC*	Low	Low	High	High	High
SC utilization	Not fully utilized	Not fully utilized	Fully utilized	Fully utilized	Fully utilized
Cost	Low	High	High	Higher	Highest
Voltage operating range	Low	Wider	Wider	More wider	More wider
Power loss	Low	High	High	Higher	Higher
Energy loss	Less	High	High	Higher	Higher
Reliability	More	Lower	Lower	Less	Less
Battery discharge time	Less	More	More	More	More
Battery cycle life	Low	High	High	Highest	Highest
Design complexity	Less	More	More	More	More

Though the passive HESS is cost-effective, the *SC* semi-active topology fulfils the benefits of both passive and full-active configurations. In this topology, the BDC will control the *SC* module and hence achieve the more extensive operating voltage range. As a result, the volumetric efficiency increases. Battery semi-active HESS is another configuration of semi-active topology. In this configuration, a huge and unstable *DC* bus voltage is expected due to the linear voltage capacity characteristics, and also the capacity of *SC* is not fully utilized. Therefore, the *SC* semi-active configuration is the optimal solution for the above-mentioned applications.

The responses of various HESS components, such as architectures, converters, power-sharing methods, modulation schemes and control techniques, are studied with the pulsed current loads to estimate and compare the performance characteristics of the chosen configuration for remote rural area applications. Here, the integration of the HESS schemes in the autonomous PV system is also discussed, and the performance investigation of these HESS topologies is carried out with the help of MATLAB Simulink models along with their control algorithms. Based on these results, comparative analyses and conclusions are presented in the subsequent sections for various HESS components. These can be used for the correct selection of architecture, converters and power-sharing methods.

Table 1 depicts the various HESS architectures used for rural electrification applications. A detailed comparative analysis among these architectures is presented by considering the various requirements of rural electrification application, such as the required number of BDC converters, volumetric efficiency, the utilization of *SC*, cost, voltage operating range, power loss, reliability, battery discharge time, battery cycle life and design complexity. There are five different configurations (passive, *SC* semi-active, battery semi-active, full-active and three-level) that are explained in Section 2, out of which the passive configuration is simple and less costly, whereas the full-active topology is the best among all configurations. However, it demands additional cost and size due to the extra controllers needed for BDCs. Therefore, a semi-active configuration is preferable, in which primary passive with active secondary ES (*SC* semi-active topology) is the optimal solution for RE applications.

4. Future Directions and Recent Trends

In addition to fulfilling the interconnection obligations established by National/International Standards, cost and efficiency are important issues for MG systems. The following trends can be seen in recent developments in MG systems.

A. Reducing Component Count

Single-stage power converter topologies with a reduced number of power semiconductor, energy storing and filtering devices are becoming increasingly popular, resulting in lower costs and higher overall power conversion efficiency than previous generations.

B. Increasing Input Operational Voltage Range

Generally, DC microgrids, particularly those powered by solar PV units, are subjected to a wide range of input fluctuations in their operating conditions. High gain converters with wide input voltage ranges, when combined with adaptive and intelligent control techniques, provide low-cost solutions for extracting the maximum amount of energy from various sources. These solutions have been shown to be reliable, robust and insensitive to changes in both the load and the input voltage and current.

C. Soft-Switched Converters

In general, hard-switching power converters have high switching losses, which makes them inefficient. Power switches in resonant converters that use ZVS and ZCS soft-switching techniques can result in significant reductions in switching losses. Because of this, soft-transition switching techniques such as zero voltage transition (ZVT) and zero current transition (ZCT) have been developed to reduce or eliminate switching losses and stresses, thereby increasing the efficiency of converters. Only a few soft-switched DC-DC converters have been proposed and are widely used in commercial applications, in part due to the high cost of additional power components and the complexity of the control circuit; however, they are deserving of further investigation.

D. Modular Structure

Small transformerless DC-DC converter modules can be used to construct a multilevel converter system that can accommodate a wide range of input voltage variations and a large power capacity, thereby improving system reliability and lowering maintenance costs.

E. Control Aspects

From the control strategies aspect, it is necessary to design a soft-switching control method with high efficiency and reliability, in which the PI control has a simple design and suitability for linear system applications. However, it is quite tricky to practice in bidirectional power flow applications since non-linearities exist in the BDCs.

The sliding mode control is applicable to both linear and nonlinear systems. This control scheme achieves fast and finite-time responses, as well as robustness against parameter variation. The disadvantage is that correct parameters and state information are required, which complicates matters. When compared to PI control, the Volterra theory is a more general approach [50].

Dynamic evolution control is implemented for specific applications to reduce dynamic state error. It can improve performance by forcing it to follow the evolution path regardless of the presence of the disturbance.

Another non-linear control approach used in BDC to achieve fast dynamic response and reference tracking characteristics is model predictive control. Although its implementation is simple, it is incapable of dealing with severe non-linear dynamic behavior.

Fuzzy logic control can be used to attain a robust response for a nonlinear and inaccurate system that is subject to uncertainty, parameter variation and load disturbance. The design of this control is also simpler than the sliding mode approach because no prior knowledge of the system parameters is required, and less measurement is required to design the controller.

Digital control is another control method for BDCs that can be used. The benefits of this control include the ability to perform smooth switching, significantly greater flexibility than analogue electronics, high immunity to EMI and enhanced process and fault monitoring via an external interface or a network connection. Boundary control can be used in time-varying circuit topologies. The benefits of this control include simple implementation, robustness and the ability to eliminate voltage and current overshoots for specific applications

5. Conclusions

In this article, detailed organization and analysis about all the architectures and converter topologies have been reported for the selection of the correct configuration and suitable type of power converters for Microgrid system applications. Various architectures proposed for the integration of various energy sources to achieve optimum performance have been reviewed along with the detailed analysis. Upon the discussion on their attributes of reviewed architectures and converter topologies, the following conclusions can be drawn:

- Non-isolated converters in DC micro grids are favored for their simple architectures, cheap weight and manufacturing costs and adaptability for low to medium power levels.
- Isolated converters in DC micro grid layouts offer reduced noise and EMI concerns, high conversion gains, compliance with most utility grid regulations and the ease of implementation of numerous output topologies with positive and/or negative voltage rails.
- When there is only one direction of power flow, unidirectional converters are preferable. In such situations, these converters can provide benefits such as simple modulation and control, reduced complexity and low cost.
- On the other hand, bidirectional converters can be used any time forward and reverse power flow is required (suitability for regenerative applications). However, they necessitate the use of sophisticated FET drivers and control units.
- Input current ripple (sometimes discontinuous) and intrinsic buck characteristics plague voltage-fed converters. Fast dynamic reaction is provided by these converters. Due to qualities such as a continuous input current with tiny ripple and intrinsic boost characteristics, current-fed topologies can be a viable alternative to voltage-fed converters. However, due to the input inductor and RHP zero, these converters have a delayed dynamic response.
- Large switching losses, strong EMI due to high dv/dt and di/dt at switching transitions, limited switching frequency, low power density and low efficiency are all common problems with hard switched converters.
- Due to zero switching losses (ZVS and ZCS), high switching frequency, better power density and high efficiency, soft switched converters can be a viable alternative to hard switched converters. However, these converters require some intricate analysis.
- Non-minimum-phase systems offer a slow dynamic response, small stability margins and often challenging control designing.
- Minimum-phase converters offer a fast dynamic response, large stability margin and easy control designing.
- There are five different HESS configurations: passive, SC semi-active, battery semi-active, full-active and three-level are available for DC micro grid applications.
- Passive HESS configuration is a simple design and requires less cost, size and volume. However, it has the disadvantages of low volumetric efficiency and low flexibility in HESS design and the incomplete utilization of SC capacity.
- The full-active topology is the best among all configurations. It has a good control effect and independent control over each ES device is possible. However, it has some disadvantages such as high initial cost, questionable robustness and large size due to the extra controllers needed for BDCs.
- The semi-active configuration has the mixed advantages of passive and active configurations. Primary passive with active secondary ES is the optimal solution for RE applications. This semi-active configuration offers advantages such as wide voltage ranges of operation, improving the volumetric efficiency and it is less expensive than full-active topology. However, the limitations are vast and an instability in DC bus voltage and a low volumetric efficiency of SC usage are expected in battery semi-active HESS.

The forthcoming Part II of this review will focus on the HESS literature review on various battery-SC HESS architectures with the mathematical models and their power

allocation strategies for the study of the conventional autonomous PV grid system. The various BDC topologies will be observed, along with detailed discussion of their classifications, control and switching strategies. The SoC balancing technologies of different ESS in solar power DC microgrids will be observed. A detailed discussion of the reviewed electronic power topologies along with their features will be presented equipped with the comparison tables to describe the various attributes such as voltage gain, circuit characteristics, the number of devices used (inductors, capacitors, windings and switches) and the applications for the reviewed non-isolated converter topologies. The overall comparison of the topologies and HESS configurations for the selection of optimal topology (including stability issues) for the specified applications will be performed as well.

Author Contributions: Conceptualization: D.R.; methodology: D.R., R.P. and M.P.; software: D.R. and R.P.; supervision: D.S., M.P. and F.L.; validations: D.R. and R.P.; data curation: A.D.; formal analysis: D.R. and R.P.; investigation: D.R. and D.S.; writing—original draft preparation: D.R. and R.P.; writing—review and editing: D.R., R.P., A.D., F.L., D.S., D.P. and B.L.N.; funding acquisition: D.S., M.P. and F.L.; project administration: D.S. All authors have read and agreed to the published version of the manuscript.

Funding: This work was supported in part by Bhaskar Advanced Solar Energy Fellowship/Internship program, IUSSTF (DST) under Grant BASE-2016 I/10" and in partnership with Zunik Energies Pvt. Ltd., under Grant Zunik-18/2020. The study of A.D., D.S. and D.P. was supported by a grant from the Ministry of Science and Higher Education of the Russian Federation (Project No. 075-15-2022-1215).

Informed Consent Statement: Not Applicable.

Data Availability Statement: Not applicable.

Acknowledgments: Authors would like to thank Zunik Energies Pvt. Ltd., the Ministry of Science and Higher Education of the Russian Federation and the International Centre for Innovations in Science, Technology and Education (ICISTE) for their financial support in the completion of this work.

Conflicts of Interest: Not applicable.

References

1. Hannah Ritchie (2019)—"Access to Energy". Available online: https://ourworldindata.org/energy-access (accessed on 6 January 2023).
2. Sachs, J.; Sawodny, O. A Two-Stage Model Predictive Control Strategy for Economic Diesel-PV-Battery Island Microgrid Operation in Rural Areas. *IEEE Trans. Sustain. Energy* **2016**, *7*, 903–913. [CrossRef]
3. Dogga, R.; Pathak, M.K. *Recent Trends in Solar PV Inverter Topologies*; Elsevier Solar Energy: Amsterdam, The Netherlands, 2019; Volume 183, pp. 57–73. ISSN 0038-092X.
4. Raveendhra, D.; Guruswamy, K.P.; Thakur, P. FPGA based 2-stage power conditioning system for PV power generation. In Proceedings of the 2013 International Conference on Power, Energy and Control (ICPEC), Dindigul, India, 6–8 February 2013; pp. 44–50.
5. Saini, T.; Raveendhra, D.; Thakur, P. Stability analysis of FPGA based perturb and observe method MPPT charge controller for solar PV system. In Proceedings of the 2013 Students Conference on Engineering and Systems (SCES), Allahabad, India, 12–14 April 2013; pp. 1–5.
6. Linssen, J.; Stenzel, P.; Fleer, J. Techno-economic analysis of photovoltaic battery systems and the influence of different consumer load profiles. *Appl. Energy* **2017**, *185*, 2019–2025. [CrossRef]
7. Hoppmann, J.; Volland, J.; Schmidt, T.S.; Hoffmann, V.H. The economic viability of battery storage for residential solar photovoltaic systems—A review and a simulation model. *Renew Sustain. Energy Rev.* **2014**, *39*, 1101–1118. [CrossRef]
8. Dufo-López, R.; Lujano-Rojas, J.M.; Bernal-Agustín, J.L. Comparison of different lead–acid battery lifetime prediction models for use in simulation of stand-alone photovoltaic systems. *Appl. Energy* **2014**, *115*, 242–253. [CrossRef]
9. Jing, W.; Lai, C.H.; Wong, W.S.H.; Wong, M.L.D. Smart hybrid energy storage for standalone PV microgrid: Optimization of battery lifespan through dynamic power allocation. In Proceedings of the Power and Energy Engineering Conference (APPEEC), IEEE PES Asia-Pacific, Beijing, China, 12–14 April 2015; Volume 2016, pp. 3–7.
10. Sidorov, D.; Muftahov, I.; Tomin, N.; Karamov, D.; Panasetsky, D.; Dreglea, A.; Liu, F.; Foley, A. A Dynamic Analysis of Energy Storage With Renewable and Diesel Generation Using Volterra Equations. *IEEE Trans. Ind. Inform.* **2020**, *16*, 3451–3459. [CrossRef]
11. Li, F.; Xie, K.; Yang, J. Optimization and Analysis of a Hybrid Energy Storage System in a Small-Scale Standalone Microgrid for Remote Area Power Supply (RAPS). *Energies* **2015**, *8*, 4802–4826. [CrossRef]

12. Mukhopadhyay, S.; Dhaouadi, R.; Takrouri, M.; Dogga, R. Supercapacitor Characterization Using Universal Adaptive Stabilization and Optimization. *IEEE Open J. Ind. Electron. Soc.* **2020**, *1*, 166–183. [CrossRef]
13. Mishra, S.K.; Kumar, M. A supervisory power management system for a hybrid microgrid with HESS. *IEEE Trans. Ind. Electron.* **2017**, *64*, 3640–3649.
14. Samani, H.; Fernando, X. Battery Current's Fluctuations Removal in Hybrid Energy Storage System Based on Optimized Control of Supercapacitor Voltage. *IEEE Embed. Syst. Lett.* **2016**, *8*, 53–56. [CrossRef]
15. Abeywardana, D.B.W.; Hredzak, B.; Agelidis, V.G. A fixed-frequency sliding mode controller for a boost-inverter-based battery-supercapacitor hybrid energy storage system. *IEEE Trans. Power Electron.* **2017**, *32*, 668–680. [CrossRef]
16. Sidorov, D.; Panasetsky, D.; Tomin, N.; Karamov, D.; Zhukov, A.; Muftahov, I.; Dreglea, A.; Liu, F.; Li, Y. Toward Zero-Emission Hybrid AC/DC Power Systems with Renewable Energy Sources and Storages: A Case Study from Lake Baikal Region. *Energies* **2020**, *13*, 1226. [CrossRef]
17. Xu, Q.; Hu, X.; Wang, P.; Xiao, J.; Tu, P.; Wen, C.; Lee, M.Y. A Decentralized Dynamic Power Sharing Strategy for Hybrid Energy Storage System in Autonomous DC Microgrid. *IEEE Trans. Ind. Electron.* **2016**, *64*, 5930–5941. [CrossRef]
18. Kim, Y.; Raghunathan, V.; Raghunathan, A. Design and Management of Battery-Supercapacitor Hybrid Electrical Energy Storage Systems for Regulation Services. *IEEE Trans. Multi-Scale Comput. Syst.* **2016**, *3*, 12–24. [CrossRef]
19. Raveendhra, D.; Dhaouadi, R.; Rehman, H.; Mukhopadhyay, S. LC Impedance Source Bi-Directional Converter with Re-duced Capacitor Voltages. *Electronics* **2020**, *9*, 1062. [CrossRef]
20. Kumar, R.; Dogga, R.; Kumar, K.N.; Vedula, V.S. Bidirectional DC-DC converters. *Pat. Off. J.* **2016**, *54*, 51–52.
21. Raveendhra, D.; Thakur, P.; Raju, B.L.N. Design and small signal analysis of solar PV fed FPGA based Closed Loop control Bi-Directional DC-DC converter. In Proceedings of the 2013 International Conference on Circuits, Power and Computing Technologies (ICCPCT), Nagercoil, India, 20–21 March 2013; pp. 283–288.
22. Narasimharaju, B.L.; Reddy, U.R.; Dogga, R. Design and analysis of voltage clamped bidirectional DC–DC converter for energy storage applications. *J. Eng.* **2018**, *2018*, 367–374. [CrossRef]
23. Narasimharaju, B.; Dubey, S.; Singh, S. Design and analysis of coupled inductor bidirectional DC–DC convertor for high-voltage diversity applications. *IET Power Electron.* **2012**, *5*, 998–1007. [CrossRef]
24. Cabrane, Z.; Ouassaid, M.; Maaroufi, M. Analysis and evaluation of battery-supercapacitor hybrid energy storage system for photovoltaic installation. *Int. J. Hydrogen Energy* **2016**, *41*, 20897–20907. [CrossRef]
25. Zheng, J.P.; Jow, T.R.; Ding, M.S. Hybrid power sources for pulsed current applications. *IEEE Trans. Aerosp. Electron. Syst.* **2001**, *37*, 288–292. [CrossRef]
26. Dougal, R.; Liu, S.; White, R. Power and life extension of battery-ultracapacitor hybrids. *IEEE Trans. Compon. Packag. Technol.* **2002**, *25*, 120–131. [CrossRef]
27. Shin, D.; Kim, Y.; Wang, Y.; Chang, N.; Pedram, M. Constant-current regulator-based battery-supercapacitor hybrid architecture for high-rate pulsed load applications. *J. Power Sources* **2012**, *205*, 516–524. [CrossRef]
28. Hredzak, B.; Agelidis, V.G.; Demetriades, G.D. A low complexity control system for a hybrid DC power source based on ultra-capacitor-lead-acid battery configuration. *IEEE Trans. Power Electron.* **2014**, *29*, 2882–2891. [CrossRef]
29. Song, Z.; Hou, J.; Hofmann, H.; Li, J.; Ouyang, M. Sliding-mode and Lyapunov function-based control for battery/supercapacitor hybrid energy storage system used in electric vehicles. *Energy* **2017**, *122*, 601–612. [CrossRef]
30. Cabrane, Z.; Ouassaid, M.; Maaroufi, M. Battery and supercapacitor for photovoltaic energy storage: A fuzzy logic management. *IET Renew. Power Gener.* **2017**, *11*, 1157–1165. [CrossRef]
31. Aktas, A.; Erhan, K.; Ozdemir, S.; Ozdemir, E. Experimental investigation of a new smart energy management algorithm for a hybrid energy storage system in smart grid applications. *Electr. Power Syst. Res.* **2017**, *144*, 185–196. [CrossRef]
32. Golchoubian, P.; Azad, N.L. Real-Time Nonlinear Model Predictive Control of a Battery–Supercapacitor Hybrid Energy Storage System in Electric Vehicles. *IEEE Trans. Veh. Technol.* **2017**, *66*, 9678–9688. [CrossRef]
33. Kuperman, A.; Aharon, I.; Malki, S.; Kara, A. Design of a Semiactive Battery-Ultracapacitor Hybrid Energy Source. *IEEE Trans. Power Electron.* **2012**, *28*, 806–815. [CrossRef]
34. Ye, C.; Miao, S.; Lei, Q.; Li, Y. Dynamic Energy Management of Hybrid Energy Storage Systems with a Hierarchical Structure. *Energies* **2016**, *9*, 395. [CrossRef]
35. Ciccarelli, F.; Clemente, G.; Iannuzzi, D. Energy storage management control based on supercapacitors using a modular multilevel inverter topology for electrical vehicles. In Proceedings of the 4th 2013 International Conference on Clean Electrical Power, ICCEP 2013, Alghero, Italy, 11–13 June 2013; pp. 170–176.
36. Kim, Y.; Koh, J.; Xie, Q.; Wang, Y.; Chang, N.; Pedram, M. A scalable and flexible hybrid energy storage system design and im-plementation. *J. Power Sour.* **2014**, *255*, 410–422. [CrossRef]
37. Ye, Y.; Cheng, K.W.E. Analysis and design of zero-current switching switched-capacitor cell balancing circuit for se-ries-connected battery/supercapacitor. *IEEE Trans. Veh. Technol.* **2018**, *67*, 948–955. [CrossRef]
38. Ma, T.; Yang, H.; Lu, L. Development of hybrid battery-supercapacitor energy storage for remote area renewable energy sys-tems. *Appl. Energy* **2015**, *153*, 56–62. [CrossRef]
39. Kuperman, A.; Aharon, I. Battery–ultracapacitor hybrids for pulsed current loads: A review. *Renew. Sustain. Energy Rev.* **2011**, *15*, 981–992. [CrossRef]

40. Zhao, C.; Yin, H.; Yang, Z.; Ma, C. A quantitative comparative study of efficiency for battery-ultracapacitor hybrid systems. In Proceedings of the IECON 2014—40th Annual Conference of the IEEE Industrial Electronics Society, Dallas, TX, USA, 29 October–1 November 2014; pp. 3076–3082.
41. Chan, M.S.W.; Chau, K.T.; Chan, C.C. Effective Charging Method for Ultracapacitors. *J. Asian Electr. Veh.* **2005**, *3*, 771–776. [CrossRef]
42. Lukic, S.; Wirasingha, S.; Rodrigues, F.; Cao, J.; Emadi, A. Power management of an ultracapacitor/battery hybris energy storge system in an HEV. In Proceedings of the IEEE Vehicle Power and Propulsion Conference, Windsor, UK, 6–8 September 2006; pp. 1–6.
43. Miller, J.; Deshpande, U. Power electronic enabled active hybrid energy storage system and its economic viability. In Proceedings of the 24th Annual IEEE Applied Power Electronics Conference and Exposition, Washington, DC, USA, 15–19 February 2009; pp. 190–198.
44. Amjadi, Z.; Williamson, S. Power electronics based solutions for plug in hybrid electric vehicle energy storage and manage-ment systems. *IEEE Trans. Ind. Electron.* **2010**, *57*, 608–616. [CrossRef]
45. Kollimalla, S.K.; Mishra, M.K.; Narasamma, N.L. Design and analysis of novel control strategy for battery and superca-pacitor storage system. *IEEE Trans. Sustain. Energy* **2014**, *5*, 1137–1144. [CrossRef]
46. Jamshidpour, E.; Saadate, S.; Poure, P. Energy management and control of a stand-alone photovoltaic/ultra capaci-tor/battery microgrid. In Proceedings of the 2015 IEEE Jordan Conference on Applied Electrical Engineering and Computing Technologies (AEECT), Amman, Jordan, 3–5 November 2015; Volume 2, pp. 1–12.
47. Akram, U.; Nadarajah, M.; Shah, R.; Milano, F. A review on rapid responsive energy storage technologies for frequency regulation in modern power systems. *Renew. Sustain. Energy Rev.* **2020**, *120*, 109626. [CrossRef]
48. Emadi, A. A new battery/ultraCapacitor hybrid energy storage system for electric, hybrid, and plug-in hybrid electric vehicles. *IEEE Trans. Power Electron.* **2012**, *27*, 122–132.
49. Jing, W.; Lai, C.H.; Wong, W.S.; Wong, M.D. A comprehensive study of battery-supercapacitor hybrid energy storage system for standalone PV power system in rural electrification. *Appl. Energy* **2018**, *224*, 340–356. [CrossRef]
50. Sidorov, D. *Integral Dynamical Models: Singularities, Signals & Control*; World Scientific Series on Nonlinear Science Series A; Chua, L.O., Ed.; World Scientific Publ. Pte Ltd.: Singapore, 2015; Volume 87.